Synthesis and interfacing of biocompatible iron oxide nanoparticles through the ferroxidase activity of *Helicobacter Pylori* ferritin

2012 Biofabrication 4 045001

(http://iopscience.iop.org/1758-5090/4/4/045001)

Biofabrication **4** (2012) 045001 (9pp) doi:10.1088/1758-5082/4/4/045001

Synthesis and interfacing of biocompatible iron oxide nanoparticles through the ferroxidase activity of *Helicobacter Pylori* ferritin

I-Liang Lee[1,3], Pei-Shan Li[2,3], Wei-Lin Yu[2] and Hsin-Hsin Shen[2,4]

[1] Department of Biological Science and Technology, National Chiao Tung University, Hsinchu 300, Taiwan
[2] Tissue Regeneration Product Technology Division, Biomedical Technology and Device Research Laboratories, Industrial Technology Research Institute, Hsinchu 310, Taiwan

E-mail: shenhsin@itri.org.tw

Received 3 May 2012
Accepted for publication 21 August 2012
Published 27 September 2012
Online at stacks.iop.org/BF/4/045001

Abstract
Ferritin is an iron storage protein that is often used to coat metallic nanoparticles, such as iron oxide nanoparticles (IONPs). However, the synthesis and biocompatibility of ferritin-coated IONPs remain unclear. Therefore, this study reports the synthesis of a ferritin gene cloned and expressed from *Helicobacter pylori* (HPFn). The ferroxidase activity of the synthase HPFn was used for the *de novo* synthesis of HPFn-coated IONPs under mild conditions. Gel filtration chromatography and transmission electron microscopy analyses demonstrated that the core–shell structure of both the 5.0 nm IONP nanocore and the 12.4 nm HPFn shell were correctly assembled. The cellular uptake of mouse macrophage cells (RAW 264.7 cells) has shown that only a few HPFn-coated IONPs (3%) were taken up after 24 h of incubation. This study compares the biocompatibility of HPFn-coated IONPs, superparamagnetic iron oxide nanoparticles (SPIOs) and ferric salt (ferric ammonium citrate) in respect to cell growth inhibition, reactive oxygen species generation and pro-inflammatory cytokine TNF-α release. Assessment results showed that the responses elicited by HPFn-coated IONPs were similar to those elicited by SPIO treatment but milder than those elicited by ferric salt treatment. This accounts for the notion that ferritin-coated IONPs are biocompatible iron agents. These findings show that the ferroxidase activity of ferritin can be used to synthesize biocompatible IONPs. The favorable properties of HPFn-coated IONPs suggest that they can be used as a non-macrophage contrast agent through further surface conjugation.

Nomenclature

IONPs	iron oxide nanoparticles
HP	Helicobacter pylori
Fn	Ferritin
HPLC	high performance liquid chromatography
SPIOs	superparamagnetic iron oxide nanoparticles
MRI	magnetic resonance imaging
TEM	transmission electron microscopy
ROS	reactive oxygen species
LPS	lipopolysaccharide

[3] These authors contributed equally to this work.
[4] Author to whom any correspondence should be addressed.

Introduction

Nanoparticles are advanced materials used in many novel applications in various disciplines. The optical properties of nanoparticles can be tuned through quantum mechanisms, such as manipulating the size, shape, composition and surface capping agent. Researchers have proposed using nanoparticles in the fields of bioimaging and biosensing because nanoparticles have optical properties that are far superior to traditional fluorophores and chromophores [1–3]. Quantum dots, gold nanoparticles and iron oxide nanoparticles (IONPs) are promising nanoparticles in this category. Quantum dots usually consist of semiconductor nanocrystals, such as CdSe and CdTe, covered with a protective shell [4]. The unique fluorescent properties of quantum dots make them suitable for acquiring multicolor images using single or multiphoton fluorescence microscopy [5]. Gold nanoparticles are synthesized from gold ions and a reducing agent followed by a capping agent to stabilize the gold nanoparticles. Resonant gold nanoparticles exhibit strong localized surface plasmon resonance with size- and shape-dependent absorption in the UV-to-NIR region [6]. Gold nanoparticles can be used as probes for chemical and biochemical sensing and fluorescent quencher applications [7]. Iron oxide nanocrystals are superparamagnetic. Many IONPs, including superparamagnetic iron oxides (SPIOs), are encapsulated by hydrophilic polymers to improve the stability and solubility. SPIOs have been used in clinical applications as a contrast agent for magnetic resonance imaging (MRI). IONPs can also function as site-specific contrast agents for detecting a broader range of pathologies in MRI [8, 9]. Unlike quantum dot and gold nanoparticles, IONPs can be safely administered in the body because they do not raise concerns of heavy metal uptake and accumulation.

Despite the huge potential of nanoparticles in biomedical applications, the principle constitution of nanoparticles (i.e. their inorganic elements) is poorly compatible with living cells. Therefore, surface coating determines the biocompatibility and performance of nanoparticles *in vivo*. Recent research into biocompatible coatings has gained much attention. In living cells, nanoparticles encounter many types of biomolecules and interact with numerous biological processes. Nanoparticles may be the subjects of chemical modification, resulting in spontaneous agglomeration and performance reduction. Some nanoparticles have an as-yet-undefined nanotoxic effect on living cells [10]. Naked nanoparticles induce oxidative stress through reactive oxygen species (ROS) generation, cellular glutathione depletion, mitochondrial injury and cell death [11]. A recent report has shown that poly(acrylic acid)-capped gold nanoparticles cause fibrinogen unfolding, pro-inflammatory cytokine release and pro-inflammatory pathway activation [12]. However, the over-stabilization of nanoparticles also raises concerns on nanopollution. Nanoparticles can enter the food chain through edible foods taken up by animals and humans, the potential consequences of nanopollution remain unclear [13]. Therefore, it is necessary to develop an interface system that can overcome these obstacles. This highlights the need for research on a biometabolizable interface to transform inorganic nanoparticles into biologically manageable materials.

Ferritin is a naturally designed nanomachine for disposing cellular irons. Ferritin sequesters iron and maintains it in a biologically safe form. Ferritin also releases stored metals in response to cell needs. Thus, ferritin plays important roles in detoxification and reservation, and is vital for maintaining iron homeostasis in living cells. Ferritin genes are ubiquitously present among bacteria, plants and animals, suggesting that they are essential genes for most organisms [14–16]. Native ferritin consists of 24 mers of homologous or heterologous subunits assembled in a spherical cage called apo-ferritin. This creates a central cavity for a 7.5 nm diameter nanocore consisting of approximately 4000 ferric ions in ferric phosphate or ferrihydrite forms [17]. Each subunit is folded into a four-α helix bundle with a di-iron center. Several negatively charged residues, such as aspartic acids and histidines, surround this di-iron center. These residues create a strong negative electrostatic potential and perform ferroxidase activities. Ferroxidase activity is required for the nucleation of the iron nanocore in the apo-ferritin. After iron core formation, auto-oxidation on the core surface is an additional pathway for iron uptake by ferritin. Iron molecules access the core through threefold or fourfold channels on the ferritin shell. The formation of IONPs by ferritin is generally regarded as a multiphase combination of ferroxidase-dependent and auto-oxidation pathways. Redox reactions accomplish the uptake or release of iron [18–20].

Although using ferritin for the engineering of nanoparticles is an interesting topic, the actual procedure for co-assembling protein–metal nanoparticles is poorly understood. The self-assembly of ferritin is a dynamic process. The protein equilibrates in several states among the subunit, the oligomers and the 24-mer ferritin cage. Encapsulated nanoparticles may leak from the ferritin cage. The metal ions binding to the protein also induce protein denaturation, leading to protein precipitation from electric charge neutralization and multivalent interaction. These unfavorable conditions make the 'native-like' ferritin-nanoparticle nanocomposites difficult to fabricate using conventional approaches. A previous study reports the cloning, expression and characterization of the ferritin gene from *Helicobacter pylori*, a bacteria living in the human stomach [21]. The cage assembly of HP-ferritin (HPFn) is highly stable, and the protein exhibits strong ferroxidase activity. Therefore, this study develops an enzymatic method for synthesizing IONPs through the ferroxidase activity of HPFn. This study also analyzes the biocompatibility and magnetic properties of this novel material.

Materials and methods

Chemicals

Sodium phosphate, tris, and sodium chloride were obtained from Merck KGaA, Darmstadt, Germany. Lysozyme, deoxyribonuclease I and ribonuclease A were purchased from Novagen, Madison, WI. Sodium dithionite, 3-(2-Pyridyl)-5,6-diphenyl-1,2,4-triazine-p,p'-disulfonic acid monosodium

salt hydrate (Ferrozine™), ferric ammonium citrate (FAC) and polyethylene glycol (average MW of 20 kDa) were obtained from Sigma Chemical Co., St. Louis, MO. Dextran (average MW of 500 kDa) was obtained from GE Healthcare, Piscataway, NJ. Resovist® was obtained from Bayer Schering AG, Berlin, Germany.

Protein purification of HPFn

The protein coding sequence of the HPFn gene was cloned from a clinical isolate strain [21]. The coding sequence was amplified by a polymerase chain reaction using the primer pair of 5'-GCGCATATGTTATCAAAAGACATC-3' and 5'-CTCGAGAGATTTCCTGCTTTTAG-3' from genomic DNA, and was ligated to pET21 (+) vector (Novagen, Madison, WI) using NdeI and XhoI restriction sites. The construct was then sequenced and transformed into BL21 *E. coli* cells. Protein expression was induced by adding 1 mM IPTG for 4 h in a mid-log culture. Cells were harvested and resuspended in a lysis buffer of 10 mM imidazole, 50 mM sodium phosphate, and 300 mM NaCl, pH 8.0 with 1 mg ml^{-1} of lysozyme, 20 μg ml^{-1} DNase I, 10 μg ml^{-1} RNase A, and 1 mM PMSF. The whole cell lysate was then centrifuged, and the supernatant was applied to N-NTA agarose (QIAGEN Inc., Alameda, CA), washed with a 20 mM imidazole buffer and eluted with 250 mM imidazole. The eluted HPFn was dialysis against a buffer of 10 mM TrisCl, 150 mM NaCl, pH 7.5 containing 1 mM EDTA and 0.2% sodium dithionite, followed by 10 mM TrisCl and 150 mM NaCl, pH 7.5. The subunit and 24-mer assembly had calculated molecular weights of 20 480 and 491 520 Da, respectively. Protein concentration was determined by a BCA protein assay (Pierce, Rockford, IL) using BSA as the standard.

Ferroxidase-mediated synthesis of iron oxide nanoparticles

The synthesis of IONPs was performed at 25 °C by stirring the following mixture: 47.5 ml of the buffer (10 mM TrisCl, 1 mM NaCl, 0.02% PEG 20000, pH 7.5), 2.5 ml of 1 mg ml^{-1} HPFn and five 0.5 ml aliquots of 10 mM ferrous chloride. Ferroxidation progressed for 5 min for each ferrous aliquot added, finally achieving a 1:5000 loading ratio of HPFn:ferrous chloride. The reaction was cooled and kept at 4 °C overnight; 1.461 g of NaCl was added to the solution and stirred for 30 min. The reaction was centrifuged at 20 000 g for 10 min. The supernatant was concentrated using a spin concentrator (VivaSpin 20, GE Healthcare, Piscataway, NJ) with a molecular weight cut-off of 100 kDa. The prepared IONPs were dialyzed against the storage buffer of 10 mM TrisCl, pH 7.4, 10 mM NaCl, 4% mannitol and 1% sucrose, and stored at 4 °C. The iron content was quantified using the Ferrozine method with FAC as the standard [22].

Characterization of iron oxide nanoparticles

HPLC analysis was performed using a Superdex 200 10/300 GL column (24 ml column gel volume; GE Healthcare, Piscataway, NJ) with a column buffer of 10 mM TrisCl, pH 7.4, 150 mM NaCl at a flow rate of 0.5 ml min^{-1}. The elution was monitored at wavelengths of 280 or 310 nm. The HPLC system was calibrated using a protein mixture of ferritin, conalbumin, carbonic anhydrase and ribonuclease A (all obtained from GE Healthcare, Piscataway, NJ).

Electron microscopy images were taken using a transmission electron microscope (TECNAI 20, Philips Electron Optics, Holland). Samples were diluted to 50 μg ml^{-1} in a buffer of 10 mM TrisCl, pH 7.4 and 150 mM NaCl, and were adsorbed onto copper grids (200 mesh with supporting formvar/carbon film; Electron Microscopy Science, PA) for 5 min. Negative stain samples were then stained with 2% phosphotungstic acid, pH 7.0, for 15 s.

In vitro biocompatibility assessment

The mouse macrophage cell line, RAW 264.7, was obtained from the Bioresource Collection and Research Center (BCRC no.: 600001; Hsinchu, Taiwan). RAW cells were maintained in Dulbecco's Modified Eagle's Medium (Invitrogen, Carlsbad, CA) supplemented with 10% fetal bovine serum and 1X of penicillin-streptomycin antibiotics (Sigma Chemical Co.) in a humidified 5% CO_2 incubator at 37 °C. Cells were seeded in a 24-well tissue culture plate at a density of 2×10^5 cells per well. HPFn-coated IONPs, Resovist® and FAC were added and incubated with the cells for 24 h. Samples were tested in triplicate. Results were presented as the mean and standard deviation. Statistical analyses were performed using ANOVA, and a p-value less than 0.05 was considered to be significant.

Cellular iron was quantified using the ferrozine assay [23]. Cells were washed with Dulbecco's PBS, 200 μl of fresh iron releasing reagent (0.75% $KMnO_4$ in 0.25M hydrochloric acid) was added and the mixture was incubated for 2 h at 65 °C. After the plate cooled to room temperature, 20 μl of iron detection solution (30 mM Ferrozine, 1M sodium ascorbate and 3M ammonium acetate) was added and incubated for 30 min. The iron quantity was measured using a SpectraMax reader (Molecular Devices, Sunnyvale, CA) at an absorption wavelength of 550 nm, with FAC as the standard.

Cell proliferation was measured by MTT assay. Fifty microliters of 5 mg ml^{-1} 3-(4,5-Dimethylthiazol-2-yl)-2,5-diphenyltetrazolium bromide (MTT; Sigma Chemical Co.) in PBS was added to each well and incubated for 1–4 h. Cell viability was measured using a SpectraMax reader (Molecular Devices, Sunnyvale, CA) at an absorption wavelength of 570 nm with a reference of 650 nm.

Cellular ROS was measured using a cell membrane-permeable reactive oxygen indicator, 5-(and-6)-chloromethyl-2',7'-dichlorodihydrofluorescein diacetate, acetyl ester (chloromethyl-H_2DCFDA; Molecular Probes Inc., Eugene, OR). Cells were resuspended in Dulbecco's PBS containing 10 mM dye and incubated for 30 min at 37 °C in a CO_2 incubator. The culture medium was refreshed, and the cells underwent an additional dye recovery period for 30 min. Treated cells were fixed by 4% paraformaldehyde and analyzed using flow cytometry (FACScan; Becton Dickinson, Franklin Lakes, NJ) with fluorescence excitation and emission wavelengths of 492 and 517 nm, respectively.

TNF-α release was measured using a sandwich ELISA kit (DuoSet mouse TNF-α, R&D systems, Minneapolis, MN)

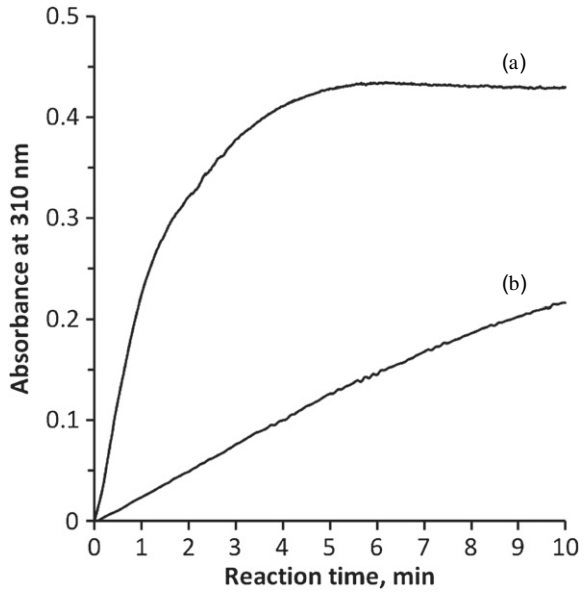

Figure 1. The reaction progression curve for ferrous oxidation under atmosphere in the presence or absence of ferritin. A fixed concentration of 0.25 mM ferrous chloride was oxidized by dissolved oxygen at room temperature (25 °C) in a ferroxidation buffer of 10 mM TrisCl, pH 7.4 and 1 mM NaCl with (trace (a)) or without (trace (b)) 0.1 μm ferritin. The increase in the absorbance at 310 nm indicates the formation of the colored reaction product of ferric oxide.

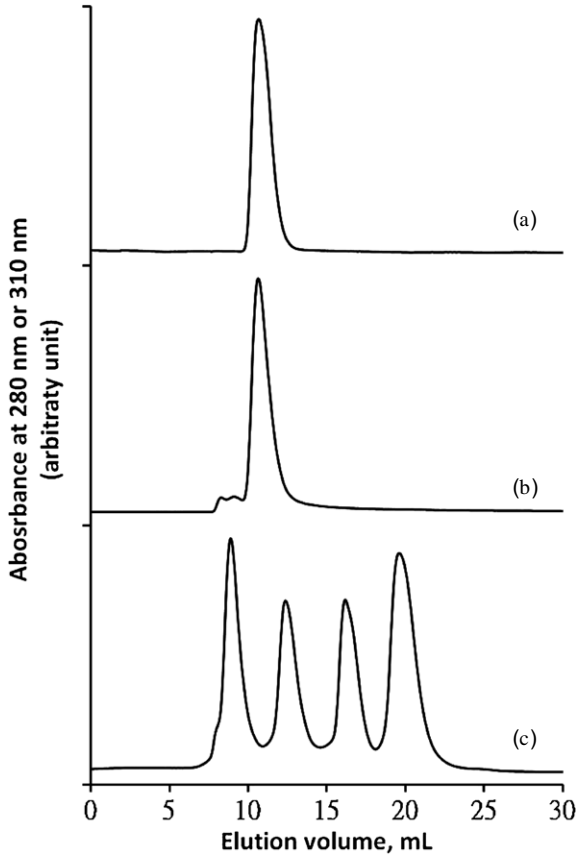

Figure 2. Gel filtration chromatographic analysis of ferritin and the synthesized IONPs. Twenty-five micrograms of HPFn (trace (a)) or 25 μg of synthesized IONPs (trace (b)) were analyzed using the HPLC system of the column of Superdex 200 (24 ml total column volume; GE Healthcare, Piscataway, NJ), the column buffer of 10 mM TrisCl, 150 mM NaCl, pH 7.4 and at a flow rate of 0.5 ml per min. The absorbances at 280 and 310 nm were set to trace the elutions of iron and protein, respectively. The HPLC system was calibrated using a protein mixture consisting of thyroglobulin (669 kDa), aldolase (158 kDa), carbonic anhydrase (29 kDa) and aprotinin (6.5 kDa), with MWs of 669, 158, 29 and 6.5 kDa, respectively (trace (c)).

following the manufacturer's instructions, and 100 μl of the culture supernatants was applied. The standard curve was created from the recombinant mouse TNF-α using a four-parameter logistic-log curve-fitting model.

Relaxivities of iron oxide nanoparticles

The longitudinal and transverse relaxivities, T1 and T2, were measured at 37 °C using a 20 MHz nuclear magnetic resonance (NMR) spectroscope (Mq20 contrast agent analyzer, Bruker Optics, MA). IONP samples were prepared in 0.75% low melting agarose in NMR tubes. The predefined plus sequences and detection modes for the T1 and T2 experiments were used, and the inversion recovery curves and the exponential decay curve were then curved fitted for the T1 and T2 values.

Result

Ferroxidase-mediated and auto-oxidation reactions

To effectively convert ferrous ions into an iron core of ferritin, two ferroxidation reactions, ferroxidase-mediated oxidation and auto-oxidation were investigated in detail. An increase in the absorbance at 310 nm was used to trace the formation of ferric oxide. Figure 1 (trace (b)) shows the auto-oxidation of ferrous chloride in a neutral aqueous buffered solution. In contrast, including 0.1 μm ferritin in the reaction significantly accelerated the rate of the ferroxidation (trace (a) versus trace (b); figure 1). Because ferroxidase-mediated oxidation and auto-oxidation are mutually exclusive, the ratio between two observed rates (defined as the present-to-absent ratio here) is useful for calculating the final iron distribution and incorporation. The ferroxidase-mediated oxidation was 5.55-fold faster than the auto-oxidation in the described reaction, in which 87% of the irons were incorporated into the ferritin cage iron through the ferroxidase-mediated pathway.

The buffer pH was vital for IONP synthesis. Table 1 shows a narrow range of pH between 6.5 and 8.0. The auto-oxidation pathway became dominant when the ratio fell below 2.0. The concentration of sodium chloride can also affect the IONP synthesis. Increasing NaCl concentration decreased the reaction yield (table 1). Trace additives, such as polyethylene glycol and dextran, have no effects, but bovine serum albumin influenced the ferroxidation reaction (table 1).

Characterization of synthesized IONPs

An optimized buffer of 10 mM TrisCl, 1 mM NaCl, 0.02% PEG and pH 7.4 was chosen. The synthesis was conducted with a 1:5000 molar ratio of HPFn:ferrous chloride, producing

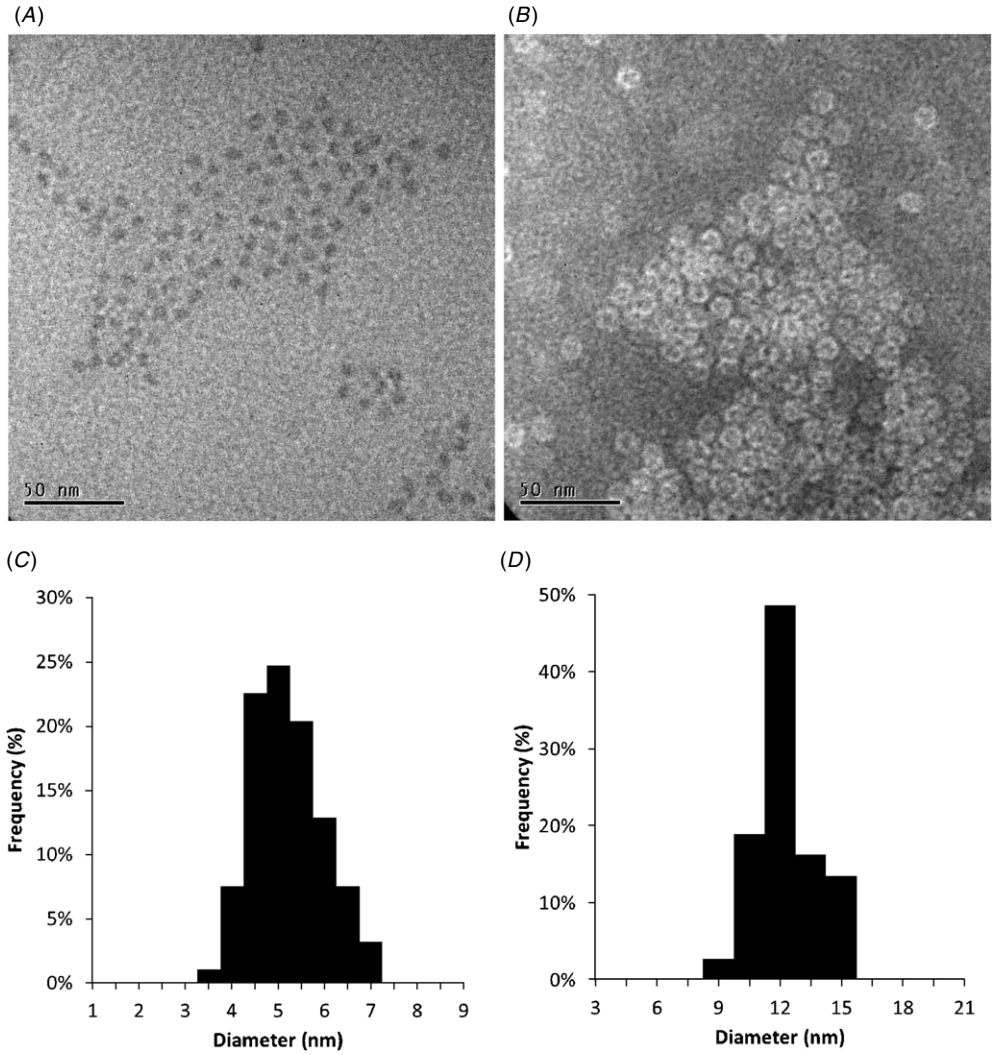

Figure 3. Transmission electron microscopy analysis of the synthesized IONPs. The sample was prepared in Dulbecco's PBS to 50 μg ml^{-1} protein and applied to a formvar-carbon film copper grid. An image was taken by TEM (*A*). The sample was also stained with 2% phosphotungstic acid, pH 7.0, for the negatively stained protein transmission electron micrograph (*B*). Size distribution of unstained ferritin-coated IONP (*C*). Size distribution of negatively stained ferritin-coated IONP (*D*).

Table 1. Effects of the buffer pH, sodium chloride and protective additives on the ferroxidase-mediated ferrous oxidation by HPFn*.

Composition	Present-to-absent ratio
10 mM NaCl with	
10 mM Bis-TrisHCl, pH 6.5	1.94
10 mM TrisHCl, pH 7.4	5.22
10 mM TrisHCl, pH 8.0	1.53
10 mM TrisHCl, pH 7.4 with	
1 mM NaCl	6.55
10 mM NaCl	5.22
100 mM NaCl	3.44
10 mM TrisHCl, pH 7.4, 1 mM NaCl with	
0.2 mg ml^{-1} BSA	3.48
0.2 mg ml^{-1} PEG 20	6.85
0.2 mg ml^{-1} Dextran 500	6.23

*0.25 mM ferrous chloride was oxidized using oxygen under an atmosphere at room temperature (25 °C) in present or absent 0.1 μm HPFn. The present-to-absent ratio is defined as the quote of reaction rates of present to absent HPFn.

approximately 3000–4000 irons per apo HPFn. The HPLC analysis revealed that most iron molecules (93%) were coeluted with ferritin in the synthesized IONPs (figure 2). The chromatographic behavior of the synthesized IONP is identical to the purified apo HPFn, confirming that the ferritin assembly remains unchanged after the ferroxidative loading of iron into the ferritin cage.

The TEM images in figure 3 show many nanoparticles in the synthesized IONPs. Image analysis by Image J (National Institutes of Health, Bethesda, MD) showed that the nanoparticles had diameters of approximately 5.0 $\pm$ 0.8 nm. In addition, negative staining showed that the protein assemblies of ferritin had diameters of 12.4 $\pm$ 2.1 nm. These measurements are consistent with the predicted results.

Iron uptake, cell growth inhibition, ROS generation and TNF-α release

The *in vitro* biocompatibility of the nanoparticles was evaluated using mouse macrophage cells (RAW 264.7). The

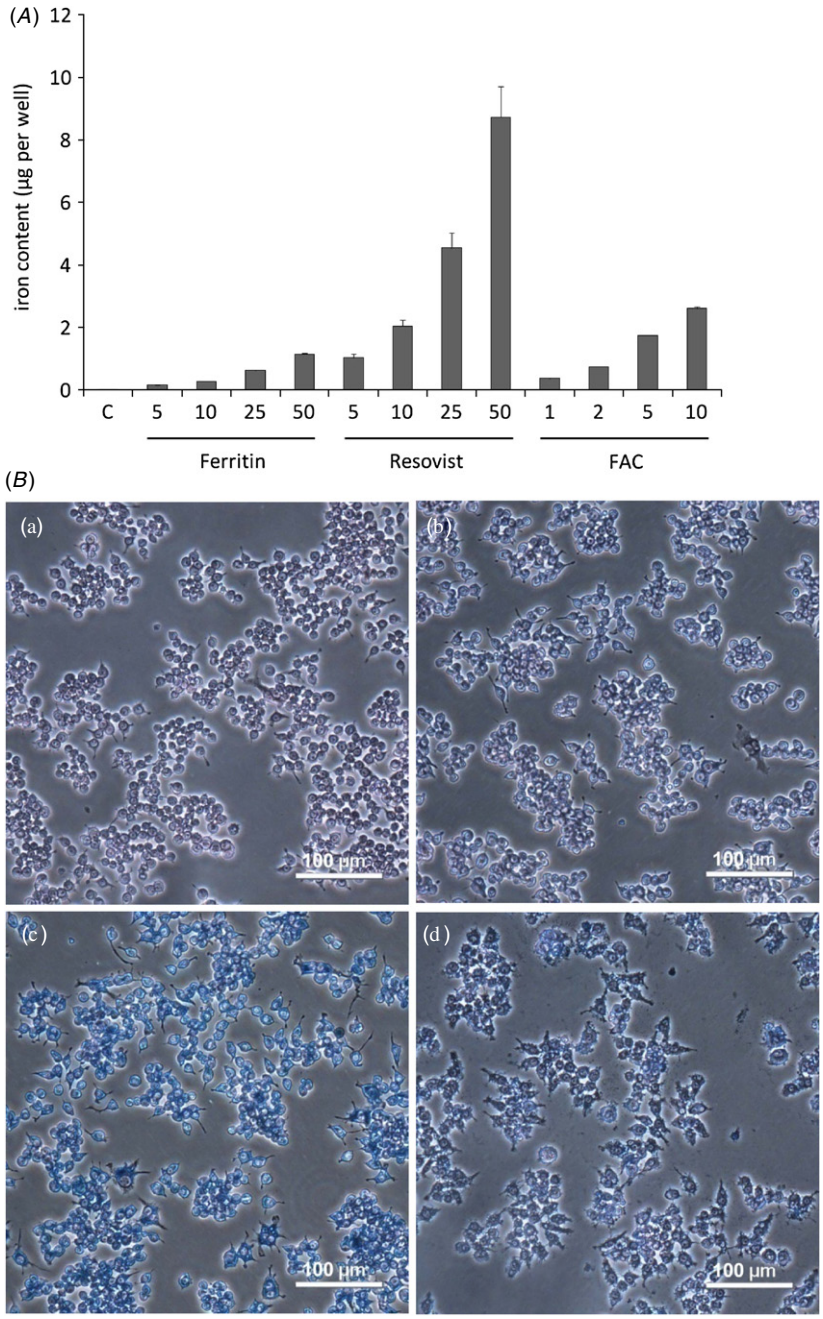

Figure 4. Uptake and accumulation of iron agents in mouse macrophage cells. RAW cells were seeded in the 24-well plate at a density of 2×10^5 cells per well. Various amounts of iron agents were added, as indicated. After 24 h incubation at 37 °C, the cellular iron was quantified using the ferrozine assay (*A*) or stained with Prussian blue (*B*). C, control; Ferritin, HPFn-coated IONPs; Resovist, Resovist®; FAC, ferric ammonium citrate. a denotes control cells; b, c and d denote 10 μg of HPFn-coated IONP, Resovist® and FAC-treated cells, respectively.

ferrozine assay revealed that RAW cells comprised only 3% of the synthesized IONPs after 24 h of incubation (figure 4(*A*)). In contrast, the uptake rates of Resovist and FAC were 19% and 31%, respectively. Prussian blue staining revealed that the intake irons accumulated in the RAW cells (figure 4(*B*)).

Excess iron loading can cause iron toxicity in iron-laden cells, possibly through ROS generation and lipid peroxidations, and can result in cell growth inhibition [10]. The growth inhibition test results were analyzed using the sensitive MTT method. Inhibitory effects were significant for the synthesized IONPs, Resovist and FAC (figure 5(*A*)). The cellular ROS level was measured using a fluorescent reagent dye. There was no significant ROS generation for RAW cells treated with these iron agents (figure 5(*B*)). This result was confirmed using lipopolysaccharides (LPS) as the positive control.

The pro-inflammatory cytokine TNF-α release from RAW cells was also measured using ELISA assay. All iron agents stimulated the TNF-α release from RAW cells at high doses. FAC was substantially more potent in this regard, because

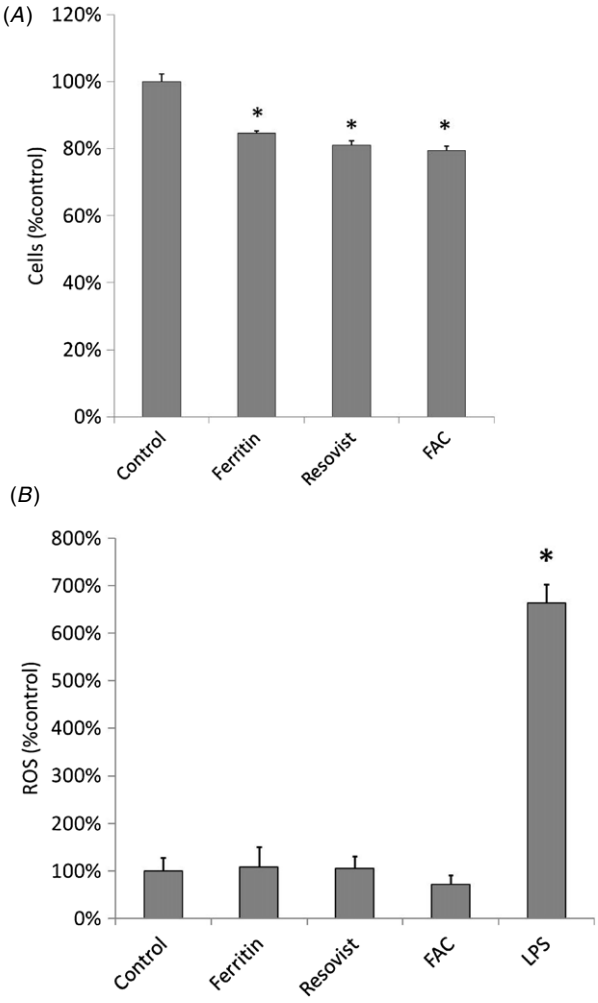

Figure 5. Effects of iron agents on cell growth and reactive oxygen species (ROS) generation. RAW cells were seeded in the 24-well plate at a density of 2×10^5 cells per well. A fixed concentration of iron agents at 100 μg ml^{-1} or LPS at 1 μg ml^{-1} in 1% FBS culture medium was added and incubated for 24 h. (*A*) Viable cells were quantified by the MTT assay. (*B*) Cellular ROS levels were measured using the chloromethyl-H_2DCFDA, a ROS indicator and flow cytometry. C, control; Ferritin, HPFn-coated IONPs; Resovist, Resovist®; FAC, ferric ammonium citrate; LPS, lipopolysaccharide.

even 2 μg caused a significant increase in TNF-α release. This amount is approximately ten times that of the synthesized ferritin and Resovist (figure 6).

Relaxivity of iron oxide nanoparticles

Finally, the magnetic properties of the synthesized IONPs were determined. The R1 and R2 values of the synthesized IONPs were 249.8 and 5779 mM^{-1}s^{-1}, respectively (figure 7). The R2/R1 ratio was 23.1, confirming that it is a T2 contrast agent capable of distorting local magnetic fields to shorten the T2 relaxation time. Thus, it is well suited to T2-weighten MR imaging.

Discussion

This study presents an enzymatic method for synthesizing ferritin-coated IONP. The intrinsic ferroxidase activity of

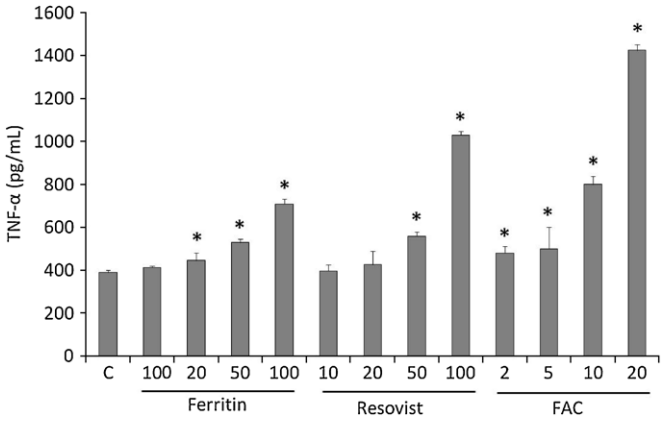

Figure 6. Effect of iron reagents on the pro-inflammatory cytokine TNF-α release. RAW cells were seeded in the 24-well plate at a density of 2×10^5 cells per well. Various concentrations of iron agents were added as indicated (in μg ml^{-1}). After 24 h incubation at 37 °C, the culture supernatants were harvested and the amounts of TNF-α were measured using the ELISA method (DuoSet mouse TNF-α, R&D Systems). C, control; Ferritin, HPFn-coated IONPs; Resovist, Resovist®; FAC, ferric ammonium citrate.

the ferritin oxidizes ferrous ions into ferric oxides, and the protein cage of the ferritin provides the size control and the interface for IONPs. This one-step synthesis and protein-coating method requires only a single reaction. Interesting, the pH of synthesis buffer seems to be vital in this regard. When the pH is 6.5 or below, most histidines located in the di-iron center of ferritin will be protonated, negatively impacting on ferroxidase-mediated oxidation. When the pH is 8.0 or above, the auto-oxidation pathway became dominant, which effectively competes with above ferroxidase-mediated oxidation. A relative narrow range of optimized pH between 6.5 and 8.0 for synthesizing ferritin-coated IONP was identified in this study.

The important conclusion of this study is that HPFn-coated IONP is a biocompatible material. The results of the growth inhibition test revealed that HPFn-coated IONPs have a lower suppressive effect than that of the free irons of FAC. The pro-inflammatory cytokine TNF-α release assay showed that the synthesized IONPs consistently have less adverse effects than FAC. However, the uptake experiment in this study showed that RAW cells took up more FAC than synthesized IONPs. In addition, the growth inhibition by HPFn-coated IONPs and FAC did not occur through an elevation in cellular ROS. Thus, the low cytotoxicity and mild TNF-α release of the HPFn-coated IONPs may be due to the low uptake rate of RAW cells. A separate analysis of a SPIO iron agent, Resovist®, showed that this biocompatible agent has a moderate iron uptake and growth inhibition effect. Resovist consists of an inner iron core and a surface layer coating of carboxydextran. Its hydrodynamic diameter is about 45–60 nm. SPIO greater than 50 nm is prone to phagocytosis and thus has a prominent uptake rate [8, 9]. No significant ROS generation was apparent in SPIO-treated RAW cells. Thus, the correlation between cell growth inhibition and cellular ROS generation is inconclusive, as is the correlation of ROS generation and TNF-α release in the present biocompatibility assessments. This may be

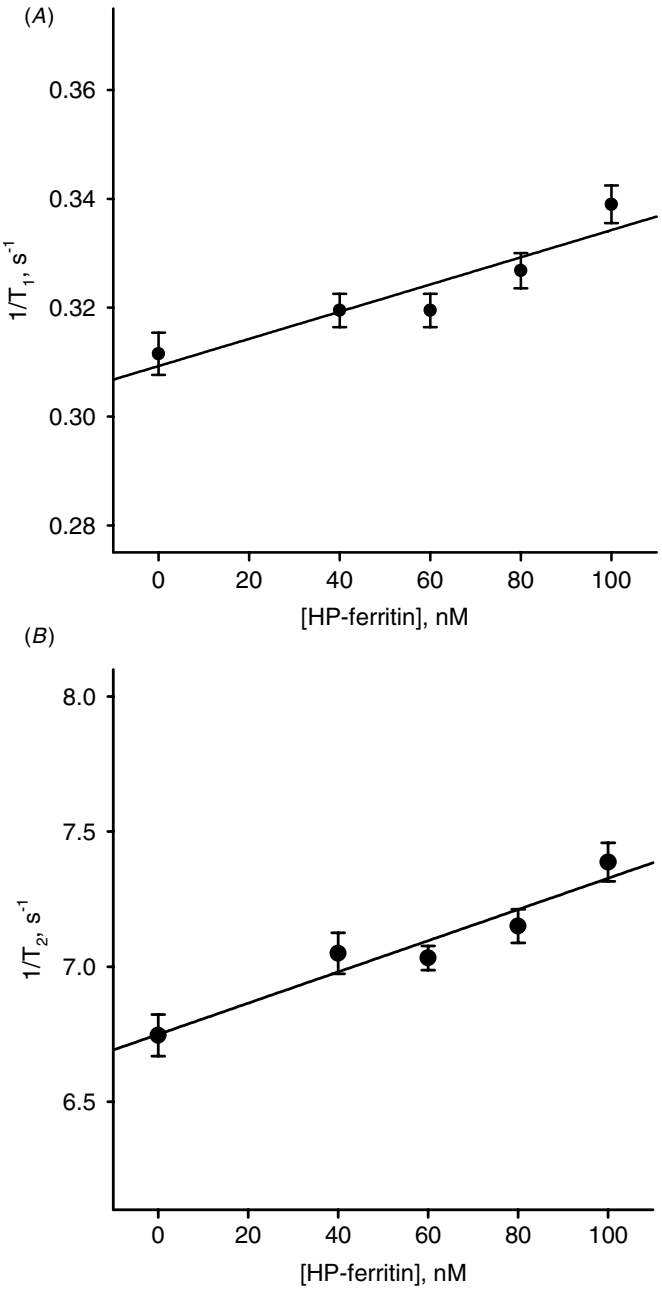

Figure 7. The molecular relaxivity of the synthesized IONPs. Various concentrations of the sample were prepared in 0.75% agarose; T1 and T2 were determined at 37 °C using a contrast agent analyzer. The R1 of 249.8 $mM^{-1}s^{-1}$ and the R2 of 5779 $mM^{-1}s^{-1}$ were obtained using linear curve fitting.

due to mechanistic differences among free iron, HPFn-coated IONP and Resovist. Investigating the receptor molecules and mapping the pathways involved can help clarify these results.

The biochemical properties of ferritin proteins from different species are distinct. Experimental data support the idea that the ferritin protein family can be used as nanoparticle-coating agents. Few ferritins have been investigated in detail in this regard. The self-assembly of *Archaeoglobus fulgidus* ferritin (AfFtn) is salt mediated. This ferritin equilibrates between dimer and 24-mer forms under physiological conditions. This dynamic assembly allows the coating of dimeric AfFtn onto gold nanoparticles [24] or IONPs [25]. The human heavy chain ferritin (rHFn) is another well-investigated protein, and rHFn-coated IONPs can be synthesized by hydrogen peroxide and heat treatment [26]. The rHFn-coated IONP can be taken up by macrophages and is a vascular macrophage-specific MRI contrast agent [27]. In contrast, this study shows that the HPFn-coated IONP decreased macrophage uptake. This may be because RAW cells have difficulty recognizing the protein surface of HPFn. Therefore, the ferritin genes from different species may provide a rich source for developing various site-specific contrast agents. A recent report presents an improved method for synthesizing and isolating high-relaxivity horse spleen ferritin-coated IONPs [28].

The ferritin-coated IONPs in this study had an iron core size of approximately 3000–5000 iron atoms and a diameter of approximately 4–6 nm. These IONPs were effective as T2 contrast agents. Despite the similarity in the iron nanocore composition, the reported R1, R2 and R2/R1 values were relatively dissimilar. The differences in magnetic properties among the reported ferritin-coated IONPs may be attributed to the size and the water accessibility of the iron nanocore [25, 28]. Therefore, the ferritin genes, the method of IONP coating and the method of isolation may significantly affect the resulting magnetic properties of the prepared IONPs.

Summary and conclusion

In conclusion, this study presents a new method of synthesizing ferritin-coated IONPs. By the ferroxidase activity, atomic iron can be directly oxidized and incorporated into the ferritin cavity to form IONPs under mild conditions. The biological characterization of HPFn-coated IONPs confirms that it is a biocompatible material without strong adverse effects. These results suggest that bacteria ferritin can be used as a new class of iron-coating agent. This type of ferritin is biologically distinct from animal ferritin because it does not participate in the endogenous iron homeostasis process in living animals. A lack of endogenous interaction suggests that this ferritin is useful for developing a site-specific contrast agent through further surface grafting and modification. Future advances in protein interface technology may ultimately provide a solution for biocompatible or even metabolizable nanoparticles.

References

[1] West J L and Halas N J 2003 Engineered nanomaterials for biophotonics applications: improving sensing, imaging, and therapeutics *Annu. Rev. Biomed. Eng.* **5** 285–92
[2] Medintz I L, Uyeda H T, Goldman E R and Mattoussi H 2005 Quantum dot bioconjugates for imaging, labelling and sensing *Nature Mater.* **4** 435–46
[3] Wang L, O'Donoghue M B and Tan W 2006 Nanoparticles for multiplex diagnostics and imaging *Nanomedicine* **1** 413–26
[4] Murray C B, Kagan C R and Bawendi M G 2000 Synthesis and characterization of monodisperse nanocrystals and close-packed nanocrystal assemblies *Annu. Rev. Mater. Sci.* **30** 545–610
[5] Larson D R, Zipfel W R, Williams R M, Clark S W, Bruchez M P, Wise F W and Webb W W 2003

Water-soluble quantum dots for multiphoton fluorescence imaging *in vivo Science* **300** 1434–6
[6] Alvarez M M, Khoury J T, Schaaff T G, Shafigullin M N, Vezmar I and Whetten R L 1997 Optical absorption spectra of nanocrystal gold molecules *J. Phys. Chem.* B **101** 3706–12
[7] Fendler J H and Hutter E 2004 Exploitation of localized surface plasmon resonance *Adv. Mater.* **16** 1685–706
[8] Wang Y X, Hussain S M and Krestin G P 2001 Superparamagnetic iron oxide contrast agents: physicochemical characteristics and applications in MR imaging *Eur. Radiol.* **11** 2319–31
[9] Mandarono G, Lodhia J, Eu P, Ferris N J, Davison R and Cowell S F 2010 Development and use of iron oxide nanoparticles: part 2. The application of iron oxide contrast agent in MRI *Biomed. Imaging Interv. J.* **6** e13
[10] Lewinski N, Colvin V and Drezek R 2008 Cytotoxicity of nanoparticles *Small* **4** 26–49
[11] Xia T, Kovochich M, Brant J, Hotze M, Sempf J, Oberley T, Sioutas C, Yeh J I, Wiesner M R and Nel A E 2006 Comparison of the abilities of ambient and manufactured nanoparticles to induce cellular toxicity according to an oxidative stress paradigm *Nano Lett.* **6** 1794–807
[12] Deng Z J, Liang M, Monteiro M, Toth I and Minchin R F 2011 Nanoparticle-induced unfolding of fibrinogen promotes Mac-1 receptor activation and inflammation *Nature Nanotechnol.* **6** 39–44
[13] Rico C M, Majumdar S, Duarte-Gardea M, Peralta-Videa J R and Gardea-Torresdey J L 2011 Interaction of nanoparticles with edible plants and their possible implications in the food chain *J. Agric. Food Chem.* **59** 3485–98
[14] Wang J and Pantopoulos K 2011 Regulation of cellular iron metabolism *Biochem. J.* **434** 365–81
[15] Aisen P and Listowsky I 1980 Iron transport and storage proteins *Annu. Rev. Biochem.* **49** 357–93
[16] Watt R K 2011 The many faces of the octahedral ferritin protein *Biometals* **24** 489–500
[17] Banyard S H, Stammers D K and Harrison P M 1978 Electron density map of apoferritin at 2.8-A resolution *Nature* **271** 282–4
[18] Le Brun N E, Wilson M T, Andrews S C, Guest J R, Harrison P M, Thomson A J and Moore G R 1993 Kinetic and structural characterization of an intermediate in the biomineralization of bacterioferritin *FEBS Lett.* **333** 197–202
[19] Pereira A S, Small W, Krebs C, Tavares P, Edmondson D E, Theil E C and Huynh B H 1998 Direct spectroscopic and kinetic evidence for the involvement of a peroxodiferric intermediate during the ferroxidase reaction in fast ferritin mineralization *Biochemistry* **37** 9871–6
[20] Douglas T and Ripoll D R 1998 Calculated electrostatic gradients in recombinant human H-chain ferritin *Protein Sci.* **7** 1083–91
[21] Huang C H, Lee I L, Yeh I J, Liao J H, Ni C L, Wu S H and Chiou S H 2010 Upregulation of a non-heme iron-containing ferritin with dual ferroxidase and DNA-binding activities in Helicobacter pylori under acid stress *J. Biochem.* **147** 535–43
[22] Viollier E, Inglett P W, Hunter K, Roychoudhury A N and Van Cappellen P 2000 The ferrozine method revisited: Fe(II)/Fe(III) determination in natural waters *Appl. Geochem.* **15** 785–90
[23] Riemer J, Hoepken H H, Czerwinska H, Robinson S R and Dringen R 2004 Colorimetric ferrozine-based assay for the quantitation of iron in cultured cells *Anal. Biochem.* **331** 370–5
[24] Swift J, Butts C A, Cheung-Lau J, Yerubandi V and Dmochowski I J 2009 Efficient self-assembly of archaeoglobus fulgidus ferritin around metallic cores *Langmuir* **25** 5219–25
[25] Sana B, Johnson E, Sheah K, Poh C L and Lim S 2010 Iron-based ferritin nanocore as a contrast agent *Biointerphases* **5** FA48–52
[26] Uchida M *et al* 2008 A human ferritin iron oxide nano-composite magnetic resonance contrast agent *Magn. Reson. Med.* **60** 1073–81
[27] Terashima M, Uchida M, Kosuge H, Tsao P S, Young M J, Conolly S M, Douglas T and McConnell M V 2011 Human ferritin cages for imaging vascular macrophages *Biomaterials* **32** 1430–7
[28] Jordan V C, Caplan M R and Bennett K M 2010 Simplified synthesis and relaxometry of magnetoferritin for magnetic resonance imaging *Magn. Reson. Med.* **64** 1260–6